なし

G．研究発表

論文発表

Fujikawa K, Iwata T, Inoue K, Akahori M, Kadotani H, Fukaya M, Watanabe M, Chang Q, Barnett EM, and Swat W. Vav2 and Vav3 as candidate disease gene for spontaneous glaucoma in mice and human. PLOS One 5:e9050 (2010)

Fujinami K, Akahori M, Fukui M, Tsunoda K, Iwata T, and Miyake Y. Stargardt disease with preserved central vision: identification of a putative novel mutation in ATP-binding cassette transporter gene. Acta Ophthalmologica (2010)

Okamoto H, Umeda S, Nozawa T, Suzuki MT, Yoshikawa Y, Matsuura ET, and Iwata T. Comparative proteomic analyses of macular versus peripheral retina in Cynomogus monkeys (Macaca fascicularis). Experimental Animal (2010)

Chi Z, Akahori, A, Obazawa M, Minami M, Noda T, Nakaya N, Tomarev S, Kawase K, Yamamoto T, Noda S, Sasaoka M, Shimazaki A, Takada Y, and Iwata T. Overexpression of optineurin E50K disrupts Rab8 interaction and leads to a progressive retinal degeneration in mice. Human Molecular Genetics (2010)

Chi Z, Yasumoto F, Sergeev Y, Minami M, Obazawa M, Kimura I, Takada Y, and Iwata T. Mutant WDR36 directly affects axon growth of retinal ganglion cells leading to progressive retinal degeneration in mice. Human Molecular Genetics (2010)

Akahori M, Tsunoda K, Miyake Y, Fukuda Y, Ishiura H, Tsuji S, Hatase T, Nakamua M, Ohde H, Itabashi T, Okamoto H, Takada Y, and Iwata T. Dominant mutations in RP1L1 gene are responsible for occult macular dystrophy. The American Journal of Human Genetics (2010)

Shen X, Ying H, Qiu Y, Park J-S, Shyam R, Chi Z-L, Iwata T, Yue BYJT. Processing of optineurin in neuronal cells. The Journal of Biological Chemistry. J Biol Chem(2011)

Zi-Bing Jin, S. Okamoto, F. Osakada, K. Homma, J. Assawachananont, Y. Hirami, T. Iwata, M. Takahashi. Modelong Retinal Degeneration Using Patient-Specific induced Pluripotent Stem Cells. PLOS One e17084(2011)

学会発表

感覚器シンポジウム（東京、2010,3）赤堀正和、加齢黄斑変性症および ポリープ状脈絡膜血管症 における全ゲノム関連解析

第49回日本網膜硝子体学会（大阪、2010,11）岩田岳、黄斑変性と黄斑ジストロトフィーの基礎研究

池　在龍、赤堀正和、安本史恵、Yuri Segreev、皆見政好、尾羽澤実、野田徹、Naoki Nakaya、Stanislav Tomarev、川瀬和秀、山本哲也、野田節子、笹岡正顕、島崎敦、木村至、高田雄一郎、岩田　岳、緑内障遺伝子 OPTN、WDR36 トランスジェニックマウスの作製とその解析

3rd Retina Research Meeting（東京、2010,12）赤堀正和、オカルト黄斑変性症原因遺伝子の解明

I. Kimura, H. Okamoto, Z.-L. Chi, M. Akahori, M. T. Suzuki, T. Iwata. Analysis of Colocalization of Rab8 and ERM Family in the Ocular Body. ARVO2010ANNUALMEETING (FortLauderdale, USA, 2010)

T. Iwata. Z.-L. Chi, M. Akahori, Y. Takada, N. Nakaya, S. Tomarev, Y. Sergeev. CHARACTERIZATION OF GLIA CELLS IN OPTN AND WDR36 TRANSGENIC MICE
19th International Congress for Eye Research. (Montreal. CANADA. 2010)
H. Okamoto. Z.-L. Chi, M. Minami, N. Terauchi, Y. Haruhata, M. Obazawa, T. Noda, M. Honda, A. Mizota, M. Tanaka, K. Matsuno, K. Tanahashi, J. Utsumi, T. Iwata.

ENRICHMENT AND ISOLATION OF LOW MOLECULAR WEIGHT PROTEIN IN PLASMA FROM PATIENTS WITH OCULAR DISEASES USING A PROTEIN SEPARATOR. 19th International Congress for Eye Research. (Montreal. CANADA. 2010)

Chi ZL. T. Toshida, K. Fujinami, Y. Miyake, A. Mizota, M. Suzuki, K. Terao, Y. Yoshikawa, J. D. Lambris, P. Olson, T. Iwata. SUPPRESSION OF DRUSEN FORMATION BY COMPSTATIN (POT-4), A PEPTIDE INHIBITOR OF C3 ACTIVATION, ON CYNOMOLGUS MONKEY WITH EARLY-ONSET MACULAR DEGENERATION. 19th International Congress for Eye Research. (Montreal. CANADA. 2010)

Chi ZL. Akahori M, Obazawa M, Minami M, Noda T, Nakaya N, Tomarev S, Kawase K, Yamamoto T, Noda S, Sasaoka M, Shimazaki A, Sergeev Y, Takada Y, Iwata T. Overexpression of mutant OPTN and WDR36 leads to a progressive retinal degeneration in mice. 50th American Society for Cell Biology. (Philadelphia. USA. 2010)

書籍

Chi Z. Yoshida T, Lambris JD, and Iwata T. Suppression of drusen formation by compstatin, a peptide inhibitor of complement C3 activation, on Cynomolgus monkey with early-onset macular degeneration. Inflammation and retinal disease:complement biology and pathology. John D. Lambris Anthony P. Adamis. 127-135. Springer. (2010)

岩田岳、「眼科と補体」、『補体への招待』木下タロウ編、189-193、メディカルビュー社(2011)

岩田　岳、「視力・資格を司る黄斑の生理機能と黄斑変性の分子メカニズム」、『実験医学』、加我君孝編、526-532、羊土社(2011)

H．知的財産権の出願・登録状況（予定を含む）

１．特許取得
なし

２．実用新案登録（平成２０－２１年度）
なし

３．その他
なし

II. 研究成果の刊行物・別刷

HMG Advance Access published May 21, 2013

Human Molecular Genetics, 2013 1–9
doi:10.1093/hmg/ddt210

Enhanced optineurin E50K–TBK1 interaction evokes protein insolubility and initiates familial primary open-angle glaucoma

Yuriko Minegishi[1], Daisuke Iejima[1], Hiroaki Kobayashi[1], Zai-Long Chi[1], Kazuhide Kawase[2], Tetsuya Yamamoto[2], Tomohisa Seki[3], Shinsuke Yuasa[3], Keiichi Fukuda[3] and Takeshi Iwata[1,*]

[1]Division of Molecular and Cellular Biology, National Institute of Sensory Organs, National Hospital Organization Tokyo Medical Center, Tokyo, Japan [2]Department of Ophthalmology, Gifu University School of Medicine, Gifu, Japan [3]Department of Cardiology, Keio University School of Medicine, Tokyo, Japan

Received March 13, 2013; Revised April 15, 2013; Accepted May 1, 2013

Glaucoma is the leading cause for blindness affecting 60 million people worldwide. The optineurin (OPTN) E50K mutation was first identified in familial primary open-angle glaucoma (POAG), the onset of which is not associated with intraocular pressure (IOP) elevation, and is classified as normal-tension glaucoma (NTG). Optineurin (OPTN) is a multifunctional protein and its mutations are associated with neurodegenerative diseases such as POAG and amyotrophic lateral sclerosis (ALS). We have previously described an E50K mutation-carrying transgenic (E50K^{tg}) mouse that exhibited glaucomatous phenotypes of decreased retinal ganglion cells (RGCs) and surrounding cell death at normal IOP. Further phenotypic analysis of these mice revealed persistent reactive gliosis and E50K mutant protein deposits in the outer plexiform layer (OPL). Over-expression of E50K in HEK293 cells indicated accumulation of insoluble OPTN in the endoplasmic reticulum (ER). This phenomenon was consistent with the results seen in neurons derived from induced pluripotent stem cells (iPSCs) from E50K mutation-carrying NTG patients. The E50K mutant strongly interacted with TANK-binding kinase 1 (TBK1), which prohibited the proper oligomerization and solubility of OPTN, both of which are important for OPTN intracellular transition. Treatment with a TBK1 inhibitor, BX795, abrogated the aberrant insolubility of the E50K mutant. Here, we delineated the intracellular dynamics of the endogenous E50K mutant protein for the first time and demonstrated how this mutation causes OPTN insolubility, in association with TBK1, to evoke POAG.

INTRODUCTION

Glaucoma is one of the world's leading cause of adult-onset blindness that causes optic nerve degeneration characterized by progressive and irreversible loss of retinal ganglion cells (RGCs) and retinal nerve fiber layer defects accompanied by the corresponding visual field damage (1). Open-angle glaucoma, the most prevalent subtype among various glaucomas, is further subdivided into two major types according to intraocular pressure (IOP). In the high-IOP type or primary open-angle glaucoma (POAG), elevated IOP due to disturbance of aqueous humor outflow in the trabecular meshwork or Schlemm's canal mechanically damages RGCs (2). In the normal-IOP type or normal-tension glaucoma (NTG), IOP elevation does not necessarily cause glaucoma, but some IOP-independent factors are thought to be involved (2). According to a population-based glaucoma survey conducted in Japan, NTG is the most prevalent subtype of glaucoma in the country (3, 4). This epidemiological study in Japan reported that the subjects' average IOP was ~15 mmHg and the POAG prevalence was almost equivalent in groups with IOP higher or lower than the average IOP (4). We have investigated the onset mechanism of the latter glaucoma subset, with lower IOP than average, as NTG. Interestingly enough, IOP-unrelated genetic mutations have been found recently in NTG (5, 6) and the Optineurin (OPTN) E50K mutation was the first one identified in familial NTG (7).

OPTN, a scaffold protein with various biological functions, has a few coiled-coil domains and a ubiquitin-binding domain

*To whom correspondence should be addressed at: Division of Molecular and Cellular Biology, National Institute of Sensory Organs, National Hospital Organization Tokyo Medical Center, 2-5-1 Higashigaoka, Meguro-ku, Tokyo 152-8902, Japan. Tel/Fax. +81 334111026; Email: iwatatakeshi@kankakuki.go.jp

at C-terminal. It associates with membrane trafficking proteins Myosin VI and Rab 8 to form Golgi ribbons and is involved in exocytosis (8, 9). And thus E50K mutation yields several phenotypes, such as fragmentation of Golgi apparatus (10), transport failure (8, 11) or apoptotic cell death (12, 13).

OPTN also participates in innate immunity response by regulating NF-κB activation and autophagy in anti-infection processes (14, 15) and via its interaction with some other proteins (16). Among the several OPTN mutations described in the original report, the role of a glutamic acid-to-lysine conversion at amino acid 50 (E50K) in NTG is well accepted worldwide (17–19). A family with a history of NTG was previously identified with the E50K mutation, and in affected members of this family, visual failure starts at about the age of 30 years (Supplementary Material, Fig. S1) and progresses to glaucoma without elevation of IOP until vision is entirely lost at about the age of 70 years (19). Recently, Maruyama *et al.* (20) identified three additional mutations in *OPTN*, a deletion in exon 5, a nonsense mutation (Q398X) and a missense mutation (E478G) that was associated with amyotrophic lateral sclerosis (ALS). Among these three mutations, the former two were recessive mutations and the latter E478G mutation was a dominant mutation, like E50K. The authors further showed the attenuation of the inhibitory effect of NF-κB activation by OPTN carrying the E478G mutation, but that the inhibitory function remained intact with the E50K mutation. Though the underlying causes of OPTN mutation-driven changes are different in POAG and ALS, it is still intriguing that OPTN plays crucial roles in neural homeostasis.

All these results suggest that the E50K mutant expression restricts retinal neural cell survival and is thus involved in the progression of POAG. The underlying molecular mechanism of how the glaucoma phenotype is evoked by a single amino acid replacement in OPTN is still unknown.

In this study, we further characterized the effects of the E50K mutation in OPTN in E50K transgenic ($E50K^{-tg}$) mice and explored the endogenous OPTN dynamics in neural cells differentiated from induced pluripotent stem cells (iPSCs) derived from NTG patients with the genetic mutation corresponding to E50K. At the molecular level, abnormal insolubility of the endogenous E50K OPTN mutant was demonstrated in this study for the first time. This insolubility was simultaneously attributed to the formation of a distinct protein complex, and to disabled oligomerization of OPTN, associated with an enhanced E50K–tank-binding kinase (TBK)1 interaction. The abnormal insolubility of the E50K mutant was rescued by treatment with a TBK1-specific inhibitor.

RESULTS

OPTN E50K transgenic mice exhibit profound gliosis in the retina

In our previous report, we showed that $E50K^{-tg}$ mice exhibited phenotypes, such as a decreased number of RGCs and progressive diminution of retinal thickness without elevation of IOP (19). Immunohistochemistry of the flat-mount retinas of $E50K^{-tg}$ mice showed persistent glial fibrillary acidic protein (GFAP)-positive dot-staining between astrocytes, compared with the staining pattern in retinas of wild-type mice (Fig. 1A and B). Evaluation of the pathological condition in age-matched wild-type and mutant mice by pathologists blinded to the sample source indicated significantly increased gliosis in the $E50K^{-tg}$ mice, compared with the wild-type mice (Fig. 1C). GFAP-positive Müller cells are known as one of the hallmarks for retinal neurodegenerative conditions, including glaucoma (21), which can be simulated by various retinal insults such as the optic nerve axonal damage, laser ablation and intravitreal injection of kainic acid (22–24). From the morphological analysis of the cells that appeared in the vertically incised retinal surface (Fig. 1D, dashed line), the GFAP-positive dots shown in the flat-mount specimen were concluded to be Müller cells, from their peculiar spindle shape (Fig. 1D, arrowheads). Reactive gliosis has been reported to be associated with retinal physical insults; thus, this phenotype in $E50K^{-tg}$ mice in the absence of physical insults was of particular interest. Therefore, in addition to the reactive gliosis in the retinas of $E50K^{-tg}$ mice, the retinal vessels were examined by *z*-axis confocal laser microscopy after tail vein injection of red fluorescent dye-conjugated isolectin. The confocal microscopy images revealed a number of gliosis scars embracing leakage of isolectin from vessels (Supplementary Material, Fig. S2A). These findings suggest that the retinas of $E50K^{-tg}$ mice are under continuous stress and are structurally vulnerable.

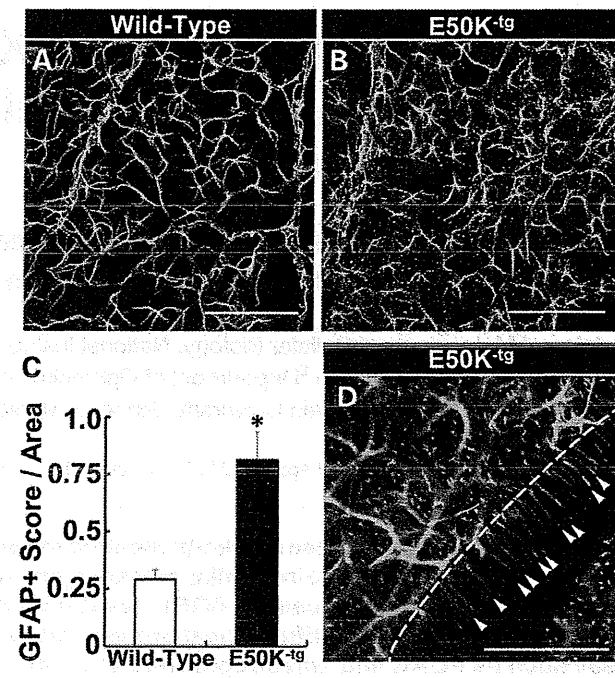

Figure 1. Persistent reactive gliosis in E50K-transgenic ($E50K^{-tg}$) mouse retinas. Representative retinal flat-mount immunohistochemistry images of anti-GFAP in (**A**) wild-type and (**B**) $E50K^{-tg}$ mice. Scale bar = 200 μm. Flat-mount specimens were analyzed (blinded evaluation) for gliosis assessment. The scores of GFAP-positive gliosis area/retinal area are plotted (data are mean ± SD; four fields of micrographs were chosen randomly and analyzed from one specimen, $n = 4$, $^*P < 0.05$). (**D**) The appearance of GFAP-positive Müller cells in $E50K^{-tg}$ mice. The dashed line indicates the border of the retinal luminal surface and the incised surface of the retina; arrowheads indicate the feet of GFAP-positive astrocytes. Scale bar = 100 μm. Some of the gliosis harbors the retinal vessel leakage (Supplementary Material, Fig. S1A).

OPTN E50K protein accumulates in the outer plexiform layer of the retinas of E50K^{-tg} mice

Considering the previous report of the deposit-like pathology in motor neurons in the ALS-associated OPTN E478G mutation (20), we also investigated the localization of the OPTN E50K protein in the retinas of E50K^{-tg} mice by immunohistochemistry. Negative control slides, treated with rabbit IgG cocktail alone, did not exhibit significant signals (Fig. 2A and B), while the retinas of E50K^{-tg} mice exhibited positive staining for OPTN in the outer plexiform layer (OPL) and the inner nuclear layer (INL), as small dot-like deposits (Fig. 2D and F, arrows). The retinas of wild-type littermates did not exhibit such a pattern (Fig. 2C and E). We designed this transgenic mouse with N-terminally HA-tagged OPTN protein, which would enable us to confirm whether the deposits include E50K mutant protein. HA-tagged E50K was mainly detected in the OPL of the retinas in E50K^{-tg} mice, which was consistent with the immunostaining results with the anti-OPTN antibody (Supplementary Material, Fig. S3D, arrows). Positive signals were not detected for OPTN in control slides in the retinas of wild-type mice and in those treated with the IgG alone (Supplementary Material, Fig. S3A–C). Thus, OPTN deposits in the retinas of E50K^{-tg} mice were caused exclusively from the expression of the E50K mutant. These pathology findings point to the capacity of the E50K mutant protein to aggregate.

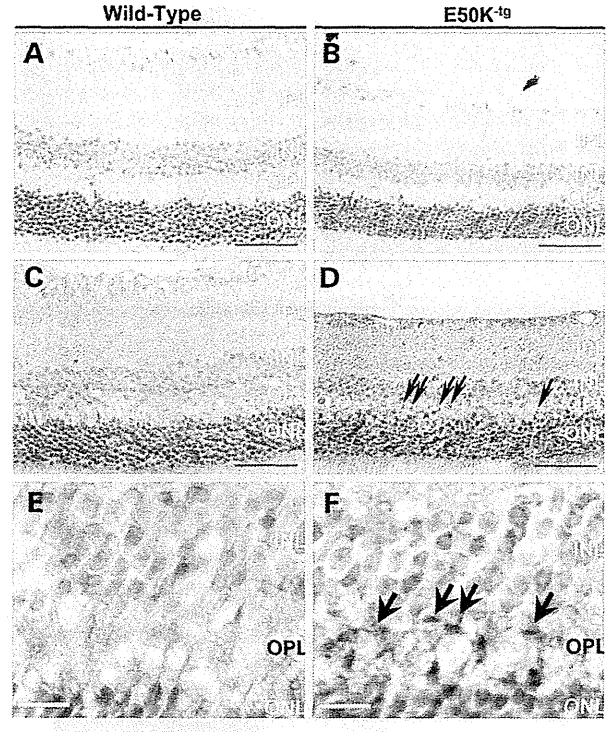

Figure 2. E50K mutant protein deposits in the retinas of E50K^{-tg} mice. (**A**) Rabbit IgG negative control for the immunohistochemistry analysis of the retina of a wild-type mouse. (**B**) Rabbit IgG negative control for the immunohistochemistry analysis of the retina of an E50K^{-tg} mouse. Both negative control slides showed minimum background staining. (**C**) Anti-OPTN immunohistochemistry of the wild-type mouse retina. Moderate OPTN signals were detected in luminal to inner layers of the retina. (**D**) Anti-OPTN immunohistochemistry of the E50K^{-tg} mouse. In addition to the moderate OPTN signals similar to that in the wild-type mouse retina, some strong deposit-like signals from INL to OPL were detected (indicated with arrows). Scale bars = 50 μm. High magnification micrograph of the retina of (**E**) wild-type and (**F**) E50K^{-tg} mice. Arrows indicate the OPTN deposit-like signals. Scale bars = 10 μm. The OPTN signals consists of, at least to some extent, the E50K^{-tg} transgene product, from the results of immunohistochemistry analysis with an anti-HA antibody (Supplementary Material, Fig. S2D). INL, inner nuclear layer; OPL, outer plexiform layer; ONL, outer nuclear layer.

Examination of induced neural cells from NTG patient-derived iPSCs indicates disturbed OPTN transition from ER to Golgi and Golgi body constriction

To clarify the cause of E50K mutant protein deposits in the retinas of E50K^{-tg} mice, we first examined the intracellular localization of wild-type OPTN and the E50K mutant by transfecting vectors encoding the two proteins fused with enhanced green fluorescent protein (EGFP) (^{EGFP}-OPTN and ^{EGFP}-E50K, respectively) into HEK 293 cells. ^{EGFP}-OPTN could be seen as small puncta widely distributed intracellularly, while ^{EGFP}-E50K was seen as larger puncta accumulated in the perinuclear region, and the Golgi body in the E50K-expressing cells was fragmented (Supplementary Material, Fig. S4B, arrowheads) as previously reported (10, 20). Since Golgi body formation and its membrane trafficking are associated with the endoplasmic reticulum (ER) (25, 26), ER structure was also examined using an ER detection kit (ER-ID, Enzo). Again, the wild-type OPTN was observed as small puncta dispersed within the cytosol (Fig. 3A), while the larger vesicles of the E50K mutant were accumulated in the perinuclear region surrounded by the ER membrane (Fig. 3B, arrows). To elucidate the intracellular localization of endogenous OPTN, we generated induced pluripotent stem cells (iPSCs) from peripheral blood mononuclear cells isolated from NTG patients with the mutation corresponding to E50K and examined OPTN localization in these cells. The pluripotency of iPSCs was confirmed by immunostaining with antibodies specific for Oct3 and Nanog, pluripotency markers (Supplementary Material, Fig. S5A). Neural induction was conducted as previously reported (27, 28) and neuronal differentiation was confirmed by staining with an antibody specific for Tuj1, a neuronal marker (Supplementary Material, Fig. S5B). iPSC-derived neural cells from NTG patients with the mutation corresponding to E50K were immunostained for OPTN and GM130, as a Golgi body marker, along with ER staining. In the iPSCs with wild-type OPTN, derived from a non-glaucoma subject, OPTN-associated vesicles were dispersed within the cells from ER to Golgi networks, in a pattern identical to that in HEK293 cells over-expressing wild-type OPTN (Fig. 3C). However, in the iPSCs from the NTG patient with the mutation corresponding to E50K, the number of OPTN-associated vesicles was decreased, compared with that in the control iPSCs, with dense aggregation in perinuclear regions and shrinkage of the ER/Golgi body (Fig. 3D). Upon microscopic examination under higher magnification, we found that wild-type OPTN frequently localized on the tips of Golgi ribbons (Fig. 3E), while the E50K OPTN mutant in iPSCs from NTG patients accumulated in the ER and Golgi body (Fig. 3F). Co-localization of wild-type OPTN and the Golgi body was

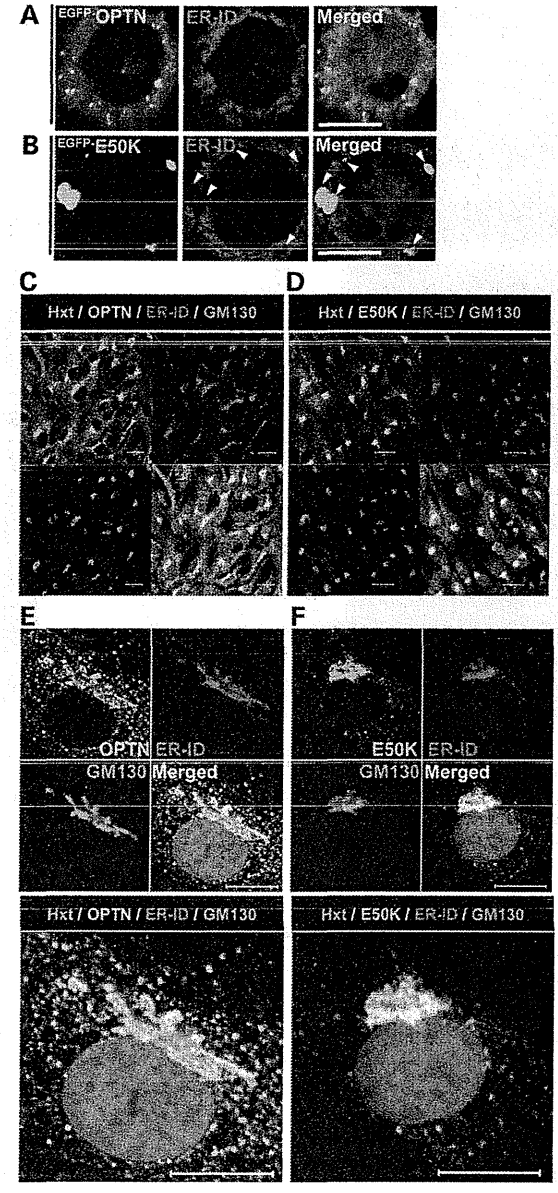

Figure 3. Distinct intracellular localization of wild-type OPTN and the E50K mutant. Intracellular localization of OPTN and E50K in over-expression studies. (**A**) ^{EGFP}-OPTN (green) and ER (red) localization 1 day after transfection. (**B**) ^{EGFP}-E50K mutant (green) and ER (red) localization 1 day after transfection. Both micrographs are shown with nuclear counter-staining with Hoechst 33342 (blue). Arrowheads indicate the E50K accumulation in the ER. Scale bars = 10 μm. iPSCs were established from iPSCs without the E50K mutation, derived from non-glaucoma subjects, as a control and with the E50K mutation, derived from glaucoma patients for endogenous analyses. Ten days after neural induction, OPTN (green), ER (red) and Golgi (magenta) co-localization were analyzed by immunocytochemistry (**C**) Endogenous OPTN localization in neural control cells or (**D**) E50K glaucoma patient-derived neural cells. OPTN signals exhibited an accumulated pattern in cells with the E50K mutation. Higher magnification of endogenous OPTN signals in (**E**) control cells and (**F**) cells with the E50K mutation. In control cells, OPTN signals (green vesicles) were localized on the tips of ribbon Golgi body, while in the cells with the E50K mutation, the number of OPTN signals was decreased and largely accumulated within the ER and to a shrunken Golgi body (shown by the white signal in merged micrographs, respectively). All scale bars = 10 μm.

frequently observed (Supplementary Material, Fig. S4A, arrow), but such a co-localization was scarce for the E50K mutant (Supplementary Material, Fig. S4B). These results indicate that the expression of the E50K mutant affects OPTN transition from ER to Golgi body prior to Golgi shrinkage/fragmentation.

Insolubility of OPTN in iPSCs and iPSC-derived neural cells from NTG patients with the mutation corresponding to E50K

While performing the over-expression experiments, we noticed that the protein amount of over-expressed E50K was decreased to half that of wild-type OPTN in HEK293T cells. A similar result has been previously reported in dermal fibroblasts from the E50K mutation-carrying patients (29). Since there was no significant difference in the mRNA levels in both groups (Supplementary Material, Fig. S6A), we speculated that E50K is more susceptible to intracellular degradation. Our previous studies have shown that OPTN is degraded by proteasomal and lysosomal pathways (30). Therefore, we first treated cells with MG132, a proteasomal inhibitor, and bafilomycin, a lysosomal inhibitor, along with cycloheximide, a protein synthesis inhibitor, to compare the amount of protein degradation. The levels of over-expressed OPTN in cells treated only with cycloheximide were lower, while co-treatment with MG132 or bafilomycin restored the OPTN protein levels, as previously reported (Supplementary Material, Fig. S7A, OPTN lanes). However, over-expressed E50K mutant protein was not restored, unlike over-expressed wild-type OPTN, upon treatment of cells with inhibitors (Supplementary Material, Fig. S7A, E50K lanes). These results indicate that there was no association between the lower levels of the E50K mutant and intracellular degradation of OPTN. We predicted that E50K might be expressed at levels comparable to the wild-type protein, but was probably insoluble and was being precipitated with the insoluble pellet (Ppt.) fraction of the cell lysate after routine cell-lysate collection. Although an equivalent amount of calnexin, a Ppt. marker, was detected in the Ppt. fraction of both wild-type- and E50K-expressing HEK293 cells, ~2- to 5-fold higher amounts of E50K protein, compared with the wild-type OPTN, was detected in the Ppt. fraction (Fig. 4A and B). The insolubilized E50K increased in an E50K expression-dependent manner (Fig. 4C). To elucidate the reason for this altered solubility of E50K mutant protein, we utilized the aforementioned iPSCs and examined the OPTN protein levels by western blotting. Although the OPTN expression was moderate in undifferentiated iPSCs, OPTN was detected in the Sup. fraction of control iPSC lysates (Fig. 4D, control 1–4), while OPTN was detected in the Ppt. fraction of iPSCs from NTG patients with the mutation corresponding to E50K (Fig. 4D, E50K 1–6). OPTN expression was significantly increased after neural induction (Fig. 4E Sup. lanes). The iPSC-derived neural cells recapitulated these results, i.e. abundant OPTN in the Ppt. fraction in E50K mutation-carrying NTG patient-derived cells (Fig. 4E, Ppt. lanes). These findings indicate that regardless of the expression levels, the E50K mutant protein exhibits higher intracellular insolubility.

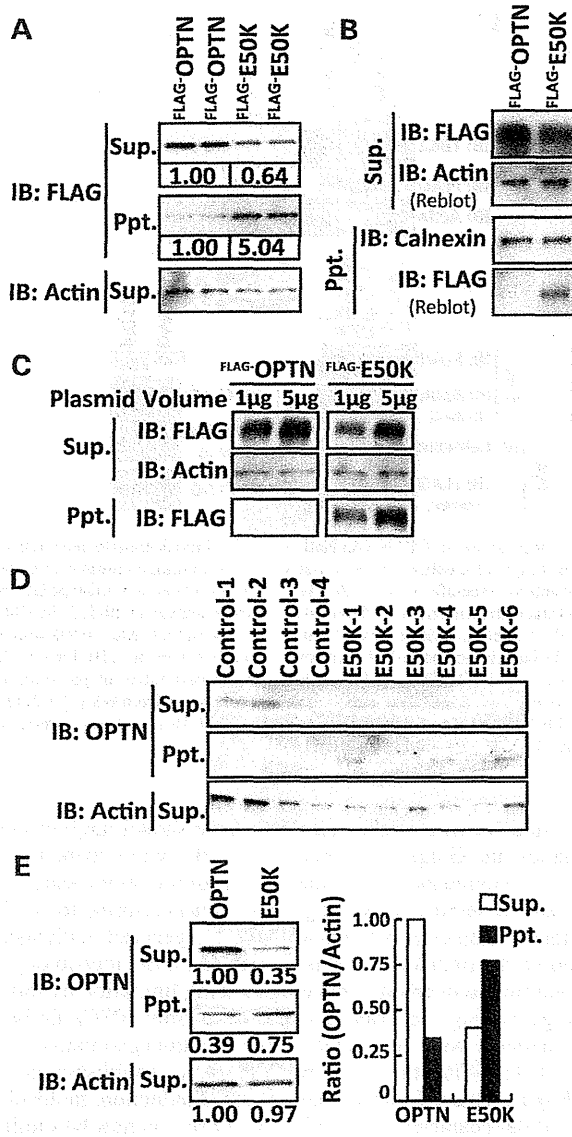

Figure 4. Distinct protein solubility of wild-type OPTN and the E50K mutant. (**A**) Wild-type OPTN and E50K expression under the same transfection condition. There were no differences in mRNA expressions under these transfection conditions (Supplementary Material, Fig. S4A). The 'Missing' E50K mutant protein was detected in the precipitated fraction (Ppt.), after supernatant (Sup.) collection. Semi-quantitative western blotting analysis was performed using Chemidoc (BioRad) with imaging software and the results are shown under each band. Approximately 2-fold reduction of E50K mutant protein in the Sup. fraction and 2- to 5-fold induction in the Ppt. fraction were observed. (**B**) Although calnexin, an ER membrane marker, is detected in both the Ppt. fraction of wild-type OPTN-expressing and E50K mutant-expressing cells, only the E50K mutant is detected in the Ppt. fraction. (**C**) The E50K mutant in the Ppt. fraction was increased in an E50K expression-dependent manner. (**D**) Endogenous expression and higher hydrophobicity of OPTN in iPSCs with the E50K mutation. Endogenous OPTN is also detected in the Ppt. fraction in iPSCs from E50K mutation-carrying NTG patients. (**E**) Abundant endogenous expression and higher hydrophobicity of OPTN in iPSC-derived neural cells 10 days after induction from E50K mutation-carrying NTG patients. Semi-quantitative western blotting analysis by Chemidoc with imaging software was performed and the results are shown under each band. The OPTN amounts in each fraction were normalized to the actin amount and then plotted. Sup., supernatant fraction, Ppt., precipitated fraction.

The enhanced affinity of TBK1 to the E50K mutant protein affects the proper oligomerization and solubility of OPTN

To elucidate the factors that affect the solubility of OPTN, we first examined the native state of wild-type OPTN and the E50K mutant. FLAG-tagged OPTN was expressed in cells and lysates were routinely prepared without detergent and separated by native-polyacrylamide gel electrophoresis (PAGE). Western blotting analysis after native-PAGE indicated more E50K-protein complexes compared with those formed by wild-type OPTN (Fig. 5A). The complexes were immunoprecipitated (IP) using an anti-FLAG antibody and then separated by SDS–PAGE, which revealed distinct binding partners of OPTN and E50K (Fig. 5B, OPTN, white arrowheads; E50K, black arrowheads). We identified each binding partner by liquid chromatography–tandem mass spectrometry (LC–MS/MS). The OPTN partner was identified as OPTN itself, indicating tight oligomerization, while the E50K protein partner was identified as TBK1, which has been previously shown to interact with OPTN by a yeast two-hybrid screening (31). Each candidate interacting partner was further confirmed by IP and western blotting (Fig. 5C and D). Intriguingly, E50K exhibited enhanced affinity to TBK1, while its self-oligomerization was largely decreased (Fig. 5C, arrowhead). Oligomerized OPTN bands clearly seen in wild-type OPTN were restored by treatment with intracellular degradation inhibitors (Supplementary Material, Fig. S7A, left panel, Oligomer lanes), indicating the importance of OPTN oligomerization in intracellular traffic and intracellular degradation. In contrast, these intracellular inhibitors had no effect on the diminished oligomerization of the E50K mutant (Supplementary Material, Fig. S7A right panel, Oligomer lanes). Treatment with a specific inhibitor treatment for TBK1, BX975 (32), was used to examine the relevance of TBK1 binding and the abnormal insolubility of the E50K mutant. BX795 treatment had no effects on the trace amounts of either wild-type OPTN (Supplementary Material, Fig. S7B) or calnexin in the Ppt. fraction (Fig. 5E); on the other hand, the amount of the insolubilized E50K mutant in the Ppt. fraction was drastically decreased by treatment with BX795 in a concentration-dependent manner. Prolonged BX795 treatment was able to restore the E50K mutant protein to the Sup. fraction (Fig. 5F). These findings indicate that the enhanced affinity of E50K for TBK1 is one of the initial pathogenic events that trigger the intracellular insolubility of OPTN leading to improper OPTN transition from the ER to the Golgi body.

DISCUSSION

The OPTN E50K mutation is the only mutation currently affirmed as causative for NTG, and therefore, it is a clinically relevant mutation for elucidating the mechanism of disease onset at a molecular level (4). Although the E50K mutation is a rare event in familial POAG, the pathology is usually progressive, leading to full blindness even under strict IOP control (Supplementary Material, Fig. S1) (17). Previous reports on E50K mutant phenotypes were focused mainly on *in vitro* models using over-expression studies. Though our initial report on the phenotypic analyses of E50K^{tg} mice was informative (19), there is a strong necessity for further establishment of the model for OPTN and its target molecules in the endogenous

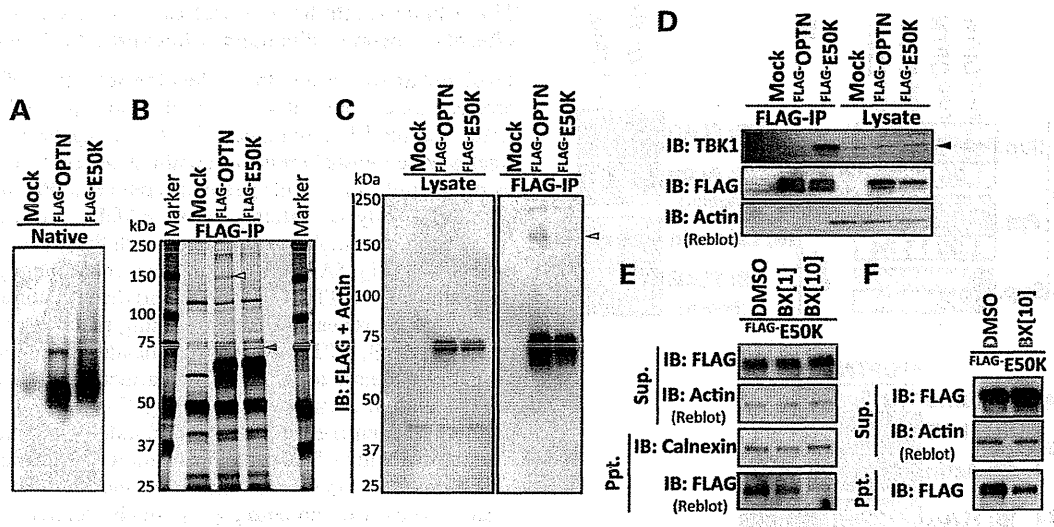

Figure 5. Constitutive interaction of the E50K mutant protein and TBK1 evokes the aberrant solubility of OPTN (**A**) Native-PAGE of mock-transfected controls, wild-type OPTN-transfected cells and E50K-transfected cells revealed the distinct protein complex formation. (**B**) Silver-staining of immunoprecipitates of mock-transfected controls, wild-type OPTN-transfected cells and E50K-transfected cells using an antibody specific for the FLAG-tag. The relevant bands, wild-type OPTN-specific binding molecule (white arrowhead) and E50K mutant-specific binding molecule (black arrowhead), were detected and further analyzed with LC–MS/MS. (**C**) Oligomerization of OPTN The band indicated with white arrowhead in (B) turned out OPTN itself, i.e. wild-type OPTN is able to oligomerize, while E50K mutant protein largely lacks this oligomerization ability. (**D**) E50K mutant and TBK1 interaction. The band indicated with black arrowhead in (B) turned out TBK1 and E50K mutant protein exhibited higher affinity to TBK1 protein than wild-type OPTN. (**E**) The treatment with BX795, a TBK1 inhibitor, decreases the aberrant precipitation of E50K mutant protein in the Ppt. fraction in a concentration-dependent manner Dimethylsulfoxide (DMSO) was used as the vehicle control and BX [1], BX [10] indicates the BX795 treatment concentrations of 1 μg/ml and 10 μg/ml, respectively, for 3 h. (**F**) Longer treatment with BX795 (6 h with 10 μg/ml) suppressed aberrant precipitation of E50K mutant protein in the Ppt. fraction and simultaneously restored E50K to the soluble fraction.

context to understand the exact molecular functions of OPTN and its mutations in glaucoma. In addition to the previously identified glaucomatous phenotypes, such as RGC loss, E50K^{-tg} mice also exhibit prominent retinal reactive gliosis with GFAP-positive Müller cells. It has been reported that GFAP-positive Müller cells can be experimentally induced in animal models mimicking glaucomatous phenotypes through various retinal insults, such as axonal damage, intravitreal injection and laser ablation (22–24). Thus, the persistent gliosis and inner layer cell death in E50K^{-tg} mice, without elevation of IOP, were of great interest, and this suggests that increased IOP is not the sole cause for POAG. The deposit-like E50K mutant protein seen in the INL of the retinas of E50K^{-tg} mice was encouraging, because similar abnormal protein inclusions are frequently found in clinical specimens of neurodegenerative tissues, including ALS (20, 33). Why E50K expression, which occurs throughout the body, only affects retinal homeostasis remains unknown. OPTN is also endogenously expressed in many other types of cells, like fibroblasts (7). In addition, most of the other cells expressing OPTN are proliferative and replaced usually within a few months, whereas the neural cells are usually non-proliferative and long-lived. We surmise that this is why the accumulation of E50K over time is critical in the pathogenesis of neurodegenerative diseases, including NTG. Though the E50K^{-tg} mice exhibit some representative neurodegenerative disease phenotypes, further investigation of the E50K accumulation in the endogenous context over time *in vivo* in the retina is needed, preferable in retinal specimens from E50K mutation-carrying NTG patient or from a mouse model, such as a site-specific knock-in mouse model.

Previous *in vitro* studies on E50K have shown large vesicle formation and Golgi fragmentation (10, 20), while there are no reports of endogenous E50K localization and behavior, especially in patient neuronal cells. In general, data pertaining to OPTN in clinical samples of patients with neurodegenerative diseases, including the retinal disease, is scarce. The iPSC technology is one solution to overcome this longstanding limitation by indirectly generating the desired target cells from iPSCs derived from patients with genetically driven neurodegenerative diseases (34). With this first report of the establishment of E50K-glaucoma iPSCs and their neuronal induction, molecular and cellular characterization of POAG onset can now be studied in the endogenous context. iPSC-derived neural cells from E50K mutation-carrying patients revealed for the first time that OPTN accumulated at the constricted Golgi body. In our current experiments, unlike the results of the E50K over-expression studies, Golgi was constricted but not fragmented. This discrepancy should be carefully examined to elucidate whether fragmentation of Golgi body is an endogenous phenotype or just an artifact induced by the over-expression. In any case, excess accumulation of E50K triggers Golgi body deformation and further deteriorates intracellular traffic, and eventually leads to cell death. It is well known that OPTN has a role in secretory vesicle transport and that E50K expression decreases the release of the neurotrophic factor NT3 (9, 35). Furthermore, prostaglandin E2 (PGE2) release via exocytosis is also decreased by E50K expression (Supplementary Material, Fig. S1B). These results indicate that due to the intracellular transport failure in cells expressing the E50K mutant, the paracrine activity for cellular protection and blood flow within the retina would also be attenuated.

Retinal vessel vulnerability in E50K^{-tg} mice is explained by these indirect extracellular E50K effects.

This study demonstrated that the E50K mutant is insoluble and is associated with the hydrophobic precipitate in lysates, compared with the wild-type OPTN, in iPSCs and iPSC-derived neural cells. Abnormal protein deposits, as shown in the retinas of the E50K^{-tg} mice, and protein hydrophobicity are frequently reported in neurodegenerative diseases (36–38). Recent reports in yeast models also supported the distinct hydrophobicities of wild-type OPTN and the E50K mutant (39). Although the prediction of isoelectric points (Compute pI/Mw, ExPASy) of wild-type OPTN and E50K do not differ (OPTN = 5.21, E50K = 5.26), their intracellular protein complex formation is considerably different. The amino acid characteristic of hydrophobic glutamate (E) against hydrophilic lysine (K) suggests that the E50K mutation is a possible charge swap mutation. E50K is located adjacent to the coiled-coil domain, which is a domain implicated in the interaction between OPTN and TBK1 (31, 15). The hydrophobicity of the E50K mutant was closely related with its enhanced interaction with TBK1, a well-known infection-responsive molecule. TBK1 induces macroautophagy by interacting with wild-type OPTN only under conditions of infection, and mediates crosstalk between innate immune response and autophagy (15). Additionally, the copy number variation of *TBK1* was associated with NTG onset (5, 6). The duplication of genes on chromosome 12q14 with familial POAG suggested that an extra copy of the *TBK1* gene and its copy number variation were responsible for NTG (40). More recently, NTG-related TBK1 mutations were also reported (41). Thus it is now well established that both *OPTN* and *TBK1* missense mutations are related with NTG onset. The abnormal physical protein interaction with TBK1 is responsible for the major cause of NTG in relation to the OPTN-E50K mutation. Together with the clinical facts, it has been reported that TBK1 has an important role in innate immunity pathways, and phosphorylated the ER-resident adaptor protein stimulator of IFN genes (STING) to enable IFN production (42, 43). Complexes of these molecules may be involved with the failure of the E50K OPTN protein to transition from ER to Golgi. Although TBK1 contributes to infection-related immunological responses, it also seems to contribute to the intracellular clearance of unnecessary components, such as by autophagy (15). Many other ophthalmic diseases, like macular diseases, are associated with abnormal protein metabolism (44); thus, the crosstalk of OPTN and TBK1 in the maintenance of intracellular clearance in retinal cells is likely to play a significant role in not only glaucomatous but also various other retinal diseases. Even though the exact function of TBK1 and the mechanism of the OPTN-TBK1 crosstalk in retinal homeostasis needs to be elucidated, compounds that abrogate the interaction between the E50K mutant and TBK1 are likely to be beneficial in the treatment of NTG patients.

Our current results pinpoint the molecular basis and concepts of NTG onset in E50K mutation-carrying patients and suggest that the RGC loss, the hallmark of glaucoma, is rather a terminal consequence of the sequential events, i.e. altered affinity of the E50K mutant inhibits self-oligomerization, leading to increased hydrophobicity, which affects downstream functions of OPTN, and eventually leads to cell death. Chronic and excessive accumulation of the E50K mutant protein recapitulated the partial neurodegenerative pathology, including reactive gliosis, vulnerability of retinal vessels and increased apoptotic cell death.

RGC loss is a hallmark of glaucoma; however, the results of this study showed that this phenomenon in E50K-NTG model is at the terminal stage of sequential abnormal events in the retina. In-depth characterization of the mutant protein in a physiologically relevant context and the proper choice/availability of a suitable animal model will help to elucidate and explore therapeutics for personalized treatment of glaucoma in the future.

MATERIALS AND METHODS

Antibodies and biochemical analysis

All the antibodies for biochemical studies were purchased from the following companies: anti-OPTN antibody (Cayman); anti-TBK1 antibody (Cell Signaling Technology); anti-FLAG (Sigma); anti-HA (Roche) and anti-Actin (Millipore). The TBK1 inhibitor, BX795, and cycloheximide were purchased from Calbiochem. Mini-PROTEAN TGX Gel and Transblot turbo system (BioRad) were used for native and SDS–PAGE western blotting according to the manufacturer's instructions. Quantitative western blotting was performed with ChemiDoc XRS+ with the Image lab software package (Biorad).

Animal experiments, preparation of retinal flat-mounts for staining and immunohistochemistry

All animal experiments were carried out in accordance with the Guide for the Care and Use of Laboratory Animals (National Institutes of Health) and the Association for Research in Vision and Ophthalmology Statement for the Use of Animals in Vision Research and approved by the Tokyo Medical Center Experimental Animal Committee. The OPTN mutant E50K^{-tg} mouse used in this study has been described previously (19). Twenty-two to 24-month-old male E50K^{-tg} mice ($n = 4$) and their littermates ($n = 4$) were sacrificed for the assessment of retinal gliosis. Both eyes were dissected and immunostained in flat-mounts as previously described (19). Briefly, dissected eyes were fixed in 2% paraformaldehyde and permeabilized with 0.1% Triton-phosphate-buffered saline (PBS). Non-specific binding was prevented by blocking with DAKO's serum-free blocking buffer, and all specimens were incubated with Alex488-conjugated anti-GFAP antibody (Millipore) for 4°C, over two nights. After radial dissection, retinas were mounted in DAKO's fluorescent mounting medium. A total of 16 retinal specimens, with four micrographs per one retinal specimen, were imaged by LSM700 confocal fluorescence microscopy (Zeiss) using a blinded method. Image analysis was conducted using the ZEN software (Zeiss) and the GFAP-positive area per retinal area was scored. The anti-OPTN (Cayman) and anti-HA (COVANCE) antibodies were used under heated antigen-retrieval conditions. Endogenous peroxidase was quenched by 3% H_2O_2 in MeOH. After primary antibody reaction for 4°C overnight, simple rabbit IgG-horse radish peroxidase (HRP) stain and mouse IgG-HRP stain for mouse tissue (Nichirei) were used as secondary HRP-conjugated polymers. After developing with 3,3′-diaminobenzidine (DAB) substrate, specimens were counter-stained with Gill's hematoxylin.

Light microscopy was performed with an Eclipse 600 microscope (Nikon).

Cell culture, transfection and immunocytochemistry

HEK293T cells were cultured in Dulbecco's modified Eagle medium (DMEM), supplemented with 10% heat-inactivated FBS. The TransIT-PRO Transfection Kit (Mirus) was used according to the manufacturer's instructions. HEK293T cells were transfected with pAC-^{GFP}, pAC-^{GFP}-OPTN and pAC-^{GFP}-E50K to assess the intracellular localization of tagged OPTN. The ER-ID Red assay kit (Enzo) was used for endoplasmic reticulum staining. Anti-GM130 and Alexa633-conjugated anti-mouse IgG antibodies were used for Golgi immunostaining. The following constructs were used for over-expression studies: pEF-BOS-^{FLAG} (45), pEF-BOS-^{FLAG}-Optineurin and pEF-BOS-^{FLAG}-E50K.

Generation of iPSC and induction of differentiation to neural cells

Human E50K mutation-carrying iPSCs and the corresponding control iPSCs were established by Sendai-viral (DNAVEC) infection as previously reported (46) from circulating T-cells in the peripheral blood of human familial glaucoma patients with fully informed consent. All procedures were approved by the Ethics Committee of National Hospital Organization Tokyo Medical Center. For maintaining the pluripotency, iPSCs were cultured in bovine fibroblast growth factor (bFGF)-containing iPSC media on Matrigel-coated culture dishes. Oct3 and Nanog were used as pluripotency markers and Tuj1 was used as the neuronal marker. Neural cell induction was performed via embryoid body formation as described previously (27, 28), utilizing the Neuron differentiation Kit (R&D Systems) in accordance with the manufacturer's procedures.

Identification of E50K-binding proteins by LC–MS/MS

Samples for LC–MS/MS analysis were prepared by preparing lysates from HEK293T cells over-expressing FLAG-tagged OPTN from pEF-BOS-^{FLAG}, pEF-BOS-^{FLAG}-Optineurin or pEF-BOS-^{FLAG}-E50K. Each lysate sample was immunoprecipitated with M2-FLAG-Agarose (Sigma) for 2 h at 4°C. The immunoprecipitated beads were washed with lysis buffer five times and then eluted with 2 M urea. The eluates were electrophoresed on 7.5% SDS–PAGE gels and the gels were silver-stained with the Silver Quest Kit (Invitrogen). The band of interest was processed for in-gel digestion for further LC–MS/MS analysis. Samples were analyzed with LCQ-DECA XP (Thermo Scientific). The obtained binding candidates and their interaction with OPTN/E50K were confirmed by immunoprecipitation and western blotting.

SUPPLEMENTARY MATERIAL

Supplementary Material is available at HMG online.

FUNDING

This work was supported by grants to T.I. by the Japanese Ministry of Health, Labour and Welfare (10103254), National Hospital Organization of Japan and the Japan Society for the Promotion of Science (09005752 to T.I., 24791885 to Y.M.). The pEF-BOS vector was a kind gift from Dr Seisuke Hattori in Kitasato University.

AUTHOR CONTRIBUTIONS

Y.M. and T.I designed the study; Y.M., D.I., H.K., Z.-L.C., H.K., performed the experiments; K.K., T.Y., T.S., S.Y., K.F. contributed new reagents/techniques; Y.M. and T.I. analyzed the data; Y.M. and T.I. wrote the paper.

REFERENCES

1 Quigley, H.A. and Broman, A.T (2006) The number of people with glaucoma worldwide in 2010 and 2020. *Br. J. Ophthalmol.*, **90**, 262–267.
2. Quigley, H.A. (2011) Glaucoma. *Lancet*, **377**, 1367–1377.
3. Suzuki, Y., Iwase, A., Araie, M., Yamamoto, T., Abe, H., Shirato, S., Kuwayama, Y , Mishima, H.K., Shimizu, H., Tomita, G *et al.* (2006) Risk factors for open-angle glaucoma in a Japanese population: the Tajimi Study *Ophthalmology*, **113**, 1613–1617
4. Iwase, A., Suzuki, Y., Araie, M., Yamamoto, T., Abe, H., Shirato, S., Kuwayama, Y., Mishima, H.K., Shimizu, H., Tomita, G. *et al.* (2004) The prevalence of primary open-angle glaucoma in Japanese: the Tajimi Study. *Ophthalmology*, **111**, 1641–1648.
5 Fingert, J.H., Robin, A.L., Stone, J.L., Roos, B.R., Davis, L.K., Scheetz, T.E., Bennett, S.R., Wassink, T.H., Kwon, Y.H., Alward, W.L. *et al.* (2011) Copy number variations on chromosome 12q14 in patients with normal tension glaucoma. *Hum. Mol. Genet.*, **20**, 2482–2494.
6. Kawase, K., Allingham, R.R., Meguro, A., Mizuki, N., Roos, B., Solivan-Timpe, F.M., Robin, A.L., Ritch, R. and Fingert, J.H. (2012) Confirmation of TBK1 duplication in normal tension glaucoma. *Exp. Eye Res.*, **96**, 178–180.
7. Rezaie, T., Child, A., Hitchings, R., Brice, G., Miller, L., Coca-Prados, M., Heon, E., Krupin, T., Ritch, R., Kreutzer, D. *et al.* (2002) Adult-onset primary open-angle glaucoma caused by mutations in optineurin. *Science*, **295**, 1077–1079
8. Sahlender, D.A., Roberts, R.C., Arden, S.D., Spudich, G., Taylor, M.J., Luzio, J.P., Kendrick-Jones, J and Buss, F. (2005) Optineurin links myosin VI to the Golgi complex and is involved in Golgi organization and exocytosis. *J. Cell Biol.*, **169**, 285–295.
9 Bond, L.M., Peden, A.A., Kendrick-Jones, J., Sellers, J.R. and Buss, F. (2011) Myosin VI and its binding partner optineurin are involved in secretory vesicle fusion at the plasma membrane. *Mol. Biol. Cell*, **22**, 54–65.
10. Park, B.C., Shen, X., Samaraweera, M. and Yue, B.Y. (2006) Studies of optineurin, a glaucoma gene: Golgi fragmentation and cell death from overexpression of wild-type and mutant optineurin in two ocular cell types. *Am. J. Pathol.*, **169**, 1976–1989.
11. Nagabhushana, A., Chalasani, M.L., Jain, N., Radha, V., Rangaraj, N., Balasubramanian, D. and Swarup, G (2010) Regulation of endocytic trafficking of transferrin receptor by optineurin and its impairment by a glaucoma-associated mutant. *BMC Cell Biol.*, **11**, 4.
12. Chalasani, M.L., Radha, V., Gupta, V., Agarwal, N., Balasubramanian, D. and Swarup, G (2007) A glaucoma-associated mutant of optineurin selectively induces death of retinal ganglion cells which is inhibited by antioxidants. *Invest. Ophthalmol. Vis. Sci.*, **48**, 1607–1614.
13. Meng, Q., Lv, J., Ge, H., Zhang, L., Xue, F., Zhu, Y. and Liu, P (2012) Overexpressed mutant optineurin(E50K) induces retinal ganglion cells apoptosis via the mitochondrial pathway *Mol. Biol. Rep.*, **39**, 5867–5873.
14. Gleason, C.E., Ordureau, A., Gourlay, R., Arthur, J.S. and Cohen, P. (2011) Polyubiquitin binding to optineurin is required for optimal activation of TANK-binding kinase 1 and production of interferon beta. *J. Biol. Chem.*, **286**, 35663–35674.
15 Wild, P., Farhan, H., McEwan, D.G., Wagner, S., Rogov, V V., Brady, N.R., Richter, B., Korac, J., Waidmann, O., Choudhary, C. *et al.* (2011)

Phosphorylation of the autophagy receptor optineurin restricts Salmonella growth. *Science*, **333**, 228–233
16. Ying, H. and Yue, B.Y (2012) Cellular and molecular biology of optineurin. *Int. Rev. Cell. Mol. Biol.*, **294**, 223–258.
17. Aung, T., Rezaie, T., Okada, K., Viswanathan, A.C., Child, A.H., Brice, G., Bhattacharya, S.S., Lehmann, O.J , Sarfarazi, M. and Hitchings, R.A. (2005) Clinical features and course of patients with glaucoma with the E50K mutation in the optineurin gene. *Invest. Ophthalmol. Vis. Sci.*, **46**, 2816–2822.
18. Hauser, M.A., Sena, D.F., Flor, J., Walter, J., Auguste, J., Larocque-Abramson, K., Graham, F., Delbono, E., Haines, J.L., Pericak-Vance, M.A. *et al.* (2006) Distribution of optineurin sequence variations in an ethnically diverse population of low-tension glaucoma patients from the United States. *J. Glaucoma*, **15**, 358–363
19. Chi, Z.L., Akahori, M., Obazawa, M., Minami, M., Noda, T., Nakaya, N., Tomarev, S., Kawase, K., Yamamoto, T., Noda, S. *et al.* (2010) Overexpression of optineurin E50K disrupts Rab8 interaction and leads to a progressive retinal degeneration in mice. *Hum. Mol. Genet.*, **19**, 2606–2615.
20. Maruyama, H., Morino, H., Ito, H., Izumi, Y., Kato, H., Watanabe, Y., Kinoshita, Y., Kamada, M., Nodera, H., Suzuki, H. *et al.* (2010) Mutations of optineurin in amyotrophic lateral sclerosis. *Nature*, **465**, 223–226.
21 Ganesh, B.S. and Chintala, S.K. (2011) Inhibition of reactive gliosis attenuates excitotoxicity-mediated death of retinal ganglion cells. *PLoS One*, **6**, e18305
22. Wurm, A., Iandiev, I., Uhlmann, S., Wiedemann, P., Reichenbach, A., Bringmann, A. and Pannicke, T (2011) Effects of ischemia-reperfusion on physiological properties of Muller glial cells in the porcine retina. *Invest. Ophthalmol. Vis. Sci.*, **52**, 3360–3367
23 Giani, A., Thanos, A., Roh, M.I., Connolly, E., Trichonas, G., Kim, I., Gragoudas, E., Vavvas, D. and Miller, J W. (2011) In vivo evaluation of laser-induced choroidal neovascularization using spectral-domain optical coherence tomography *Invest. Ophthalmol. Vis. Sci.*, **52**, 3880–3887
24. Ueda, K., Nakahara, T., Hoshino, M., Mori, A., Sakamoto, K. and Ishii, K. (2010) Retinal blood vessels are damaged in a rat model of NMDA-induced retinal degeneration. *Neurosci. Lett.*, **485**, 55–59
25 Lasiecka, Z.M. and Winckler, B. (2011) Mechanisms of polarized membrane trafficking in neurons – focusing in on endosomes. *Mol. Cell. Neurosci.*, **48**, 278–287
26. Farhan, H., Freissmuth, M. and Sitte, H.H. (2006) Oligomerization of neurotransmitter transporters: a ticket from the endoplasmic reticulum to the plasma membrane. *Handb. Exp. Pharmacol.*, **175**, 233–249
27. Tsuji, O., Miura, K., Okada, Y., Fujiyoshi, K., Mukaino, M., Nagoshi, N., Kitamura, K., Kumagai, G., Nishino, M., Tomisato, S. *et al.* (2010) Therapeutic potential of appropriately evaluated safe-induced pluripotent stem cells for spinal cord injury. *Proc. Natl Acad. Sci. USA*, **107**, 12704–12709.
28. Tucker, B.A., Scheetz, T.E., Mullins, R.F., DeLuca, A.P., Hoffmann, J.M., Johnston, R.M., Jacobson, S.G., Sheffield, V.C. and Stone, E.M. (2011) Exome sequencing and analysis of induced pluripotent stem cells identify the cilia-related gene male germ cell-associated kinase (MAK) as a cause of retinitis pigmentosa. *Proc. Natl Acad. Sci. USA*, **108**, E569–576.
29 Sarfarazi, M. and Rezaie, T. (2003) Optineurin in primary open angle glaucoma. *Ophthalmol. Clin. North Am.*, **16**, 529–541
30. Shen, X., Ying, H., Qiu, Y., Park, J.S., Shyam, R., Chi, Z.L., Iwata, T and Yue, B.Y (2011) Processing of optineurin in neuronal cells. *J. Biol. Chem.*, **286**, 3618–3629.
31 Morton, S., Hesson, L., Peggie, M. and Cohen, P (2008) Enhanced binding of TBK1 by an optineurin mutant that causes a familial form of primary open angle glaucoma. *FEBS Lett.*, **582**, 997–1002.
32. Clark, K., Plater, L., Peggie, M. and Cohen, P (2009) Use of the pharmacological inhibitor BX795 to study the regulation and physiological roles of TBK1 and IkappaB kinase epsilon: a distinct upstream kinase mediates Ser-172 phosphorylation and activation. *J Biol. Chem.*, **284**, 14136–14146.
33. Ito, H., Nakamura, M., Komure, O., Ayaki, T., Wate, R., Maruyama, H., Nakamura, Y., Fujita, K., Kaneko, S., Okamoto, Y *et al.* (2011) Clinicopathologic study on an ALS family with a heterozygous E478G optineurin mutation. *Acta Neuropathol.*, **122**, 223–229.
34. Imaizumi, Y., Okada, Y., Akamatsu, W., Koike, M., Kuzumaki, N , Hayakawa, H., Nihira, T., Kobayashi, T., Ohyama, M., Sato, S. *et al.* (2012) Mitochondrial dysfunction associated with increased oxidative stress and alpha-synuclein accumulation in PARK2 iPSC-derived neurons and postmortem brain tissue. *Mol. Brain*, **5**, 35
35. Sippl, C., Bosserhoff, A.K., Fischer, D. and Tamm, E.R. (2011) Depletion of optineurin in RGC-5 cells derived from retinal neurons causes apoptosis and reduces the secretion of neurotrophins. *Exp. Eye Res.*, **93**, 669–680.
36. Nukina, N., Kosik, K.S. and Selkoe, D.J. (1987) Recognition of Alzheimer paired helical filaments by monoclonal neurofilament antibodies is due to crossreaction with tau protein. *Proc. Natl Acad. Sci. USA*, **84**, 3415–3419
37 Hoffner, G., Kahlem, P and Djian, P (2002) Perinuclear localization of huntingtin as a consequence of its binding to microtubules through an interaction with beta-tubulin. relevance to Huntington's disease. *J Cell Sci.*, **115**, 941–948.
38. LaVoie, M.J., Ostaszewski, B.L., Weihofen, A., Schlossmacher, M.G. and Selkoe, D.J (2005) Dopamine covalently modifies and functionally inactivates parkin. *Nat. Med.*, **11**, 1214–1221
39 Kryndushkin, D., Ihrke, G., Piermartiri, T.C. and Shewmaker, F (2012) A yeast model of optineurin proteinopathy reveals a unique aggregation pattern associated with cellular toxicity *Mol. Microbiol.*, **86**, 1531–1547
40. Fingert, J.H., Darbro, B.W., Qian, Q., Van Rheeden, R., Miller, K., Riker, M., Solivan-Timpe, F., Roos, B.R., Robin, A.L. and Mullins, R.F (2013) TBK1 and flanking genes in human retina. *Ophthalmic Genet.* , doi.10.3109/13816810.2013 768674.
41 Seo, S., Solivan-Timpe, F , Roos, B.R., Robin, A.L., Stone, E.M., Kwon, Y.H., Alward, W.L. and Fingert, J.H. (2013) Identification of proteins that interact with TANK binding kinase 1 and testing for mutations associated with glaucoma. *Curr Eye Res.*, **38**, 310–315.
42. Saitoh, T., Fujita, N., Hayashi, T., Takahara, K., Satoh, T., Lee, H., Matsunaga, K., Kageyama, S., Omori, H., Noda, T *et al.* (2009) Atg9a controls dsDNA-driven dynamic translocation of STING and the innate immune response. *Proc. Natl Acad. Sci. USA*, **106**, 20842–20846.
43 Tanaka, Y. and Chen, Z.J (2012) STING specifies IRF3 phosphorylation by TBK1 in the cytosolic DNA signaling pathway *Sci. Signal.*, **5**, ra20.
44. Shaw, P.X., Zhang, L., Zhang, M., Du, H., Zhao, L., Lee, C., Grob, S., Lim, S.L., Hughes, G., Lee, J *et al.* (2012) Complement factor H genotypes impact risk of age-related macular degeneration by interaction with oxidized phospholipids. *Proc. Natl Acad. Sci. USA*, **109**, 13757–13762.
45 Mizushima, S. and Nagata, S. (1990) pEF-BOS, a powerful mammalian expression vector *Nucleic Acids Res.*, **18**, 5322.
46. Seki, T., Yuasa, S., Oda, M., Egashira, T., Yae, K., Kusumoto, D., Nakata, H., Tohyama, S., Hashimoto, H., Kodaira, M. *et al.* (2010) Generation of induced pluripotent stem cells from human terminally differentiated circulating T cells. *Cell Stem Cell*, **7**, 11–14.

CLINICAL CHARACTERISTICS OF OCCULT MACULAR DYSTROPHY IN FAMILY WITH MUTATION OF *RP1L1* GENE

KAZUSHIGE TSUNODA, MD, PHD,* TOMOAKI USUI, MD, PHD,†‡ TETSUHISA HATASE, MD, PHD,† SATOSHI YAMAI, MD,§ KAORU FUJINAMI, MD,* GEN HANAZONO, MD, PHD,* KEI SHINODA, MD, PHD,*¶ HISAO OHDE, MD, PHD,** MASAKAZU AKAHORI, PHD,* TAKESHI IWATA, PHD,* YOZO MIYAKE, MD, PHD*††

Purpose: To report the clinical characteristics of occult macular dystrophy (OMD) in members of one family with a mutation of the *RP1L1* gene.

Methods: Fourteen members with a p.Arg45Trp mutation in the *RP1L1* gene were examined. The visual acuity, visual fields, fundus photographs, fluorescein angiograms, full-field electroretinograms, multifocal electroretinograms, and optical coherence tomographic images were examined. The clinical symptoms and signs and course of the disease were documented.

Results: All the members with the *RP1L1* mutation except one woman had ocular symptoms and signs of OMD. The fundus was normal in all the patients during the entire follow-up period except in one patient with diabetic retinopathy. Optical coherence tomography detected the early morphologic abnormalities both in the photoreceptor inner/outer segment line and cone outer segment tip line. However, the multifocal electroretinograms were more reliable in detecting minimal macular dysfunction at an early stage of OMD.

Conclusion: The abnormalities in the multifocal electroretinograms and optical coherence tomography observed in the OMD patients of different durations strongly support the contribution of *RP1L1* mutation to the presence of this disease.

RETINA 32:1135–1147, 2012

Occult macular dystrophy (OMD) was first described by Miyake et al[1] to be a hereditary macular dystrophy without visible fundus abnormalities. Patients with OMD are characterized by a progressive decrease of visual acuity with normal-appearing fundus and normal fluorescein angiograms (FA). The important signs of OMD are normal full-field electroretinograms (ERGs) but abnormal focal macular ERGs and multifocal electroretinograms (mfERGs) also exist. These findings indicated that the retinal dysfunction was confined to the macula.[1–5] Optical coherence tomography (OCT) showed structural changes in the outer nuclear and photoreceptor layers.[6–11]

Recently, we found that dominant mutations in the *RP1L1* gene were responsible for OMD.[12] The *RP1L1* gene was originally cloned as a gene derived from common ancestors as a retinitis pigmentosa 1 (*RP1*) gene, which is responsible for 5–10% of autosomal dominant retinitis pigmentosa worldwide, on the same Chromosome 8.[13–17] A number of attempts have been made to identify mutations in *RP1L1* in various retinitis pigmentosa patients with no success. An immunohistochemical study on cynomolgus monkeys showed that *RP1L1* was expressed in rod and cone photoreceptors, and *RP1L1* is thought to play important roles in the morphogenesis of the photoreceptors.[13,18] Heterozygous *RP1L1* knockout mice were reported to be normal, whereas homozygous knockout mice develop subtle retinal degeneration.[18] However, the RP1L1 protein has a very low degree of overall sequence

From the *Laboratory of Visual Physiology, National Institute of Sensory Organs, Tokyo, Japan, †Division of Ophthalmology and Visual Science, Graduate School of Medical and Dental Sciences, Niigata University, Niigata, Japan; ‡Akiba Eye Clinic, Niigata, Japan; §Department of Ophthalmology, Sado General Hospital, Niigata, Japan; ¶Department of Ophthalmology, School of Medicine, Teikyo University, Tokyo, Japan; **Department of Ophthalmology, School of Medicine, Keio University, Tokyo, Japan; and ††Aichi Medical University, Aichi, Japan.

The authors have no financial interest or conflicts of interest.

Supported in part by research grants from the Ministry of Health, Labor and Welfare, Japan and Japan Society for the Promotion of Science, Japan.

Reprint requests: Kazushige Tsunoda, Laboratory of Visual Physiology, National Institute of Sensory Organs, 2-5-1 Higashigaoka, Meguro-ku, Tokyo 152-8902, Japan, e-mail: tsunodakazushige@kankakuki.go.jp

identity (39%) between humans and mice compared with the average values of sequence similarity observed between humans and mice proteins. The results of linkage studies have strongly supported the contribution of *RP1L1* mutations to the presence of this disease,[12] but the function of *RP1L1* in the human retina has not been completely determined.

A large number of cases of OMD have been reported[7,10,19]; however, we did not always find the same mutations in sporadic cases or in small families, which had less than three affected members. This led us to hypothesize that several independent mutations can lead to the phenotype of OMD, that is, OMD is not a single disease caused by a specific gene mutation, but may represent different diseases with similar retinal dysfunctions.

Thus, the aim of this study was to determine the characteristics of OMD by investigating the phenotypes of patients with the *RP1L1* mutation from a single Japanese family.

Patients and Methods

We investigated 19 members from a single Japanese family. A homozygous mutation, p.Arg45Trp in the *RP1L1* gene, was confirmed in 14 members,[12] and 13 of the 14 were diagnosed with OMD. Among the 14 members with a mutation in the *RP1L1* gene, 11 were followed-up at the Niigata University in Niigata, Japan. The other three were examined at the National Institute of Sensory Organs in Tokyo, Japan. Each member had a complete ophthalmic examination including best-corrected visual acuity (BCVA), refraction, perimetry, fundus photography, FA, full-field ERGs,[20] mfERGs,[21] and OCT. The visual fields were determined by Goldmann perimetry or by Humphrey Visual Field Analyzer (Model 750i; Carl Zeiss Meditec, Inc, Dublin, CA). The SITA Standard strategy was used with the 30-2 program or the 10-2 program for the Humphrey Visual Field Analyzer.

Electroretinograms were used to assess the retinal function under both scotopic and photopic conditions.[22] Full-field ERGs were recorded using the International Society of Clinical Electrophysiology and Vision standard protocol. Multifactorial electroretinograms were recorded with the Visual Evoked Response Imaging System (VERIS science 4.1; EDI, San Mateo, CA). A Burian–Allen bipolar contact lens electrode was used to record the mfERGs. The visual stimuli consisted of 61 or 103 hexagonal elements with an overall subtense of approximately 60°. The luminance of each hexagon was independently modulated between black (3.5 cd/m^2) and white (138.0 cd/m^2) according to a binary m-sequence at 75 Hz. The surround luminance was 70.8 cd/m^2.

The OCT images were obtained with a spectral-domain OCT (HD-OCT; Carl Zeiss Meditec or a 3D-OCT-1000, Mark II; Topcon) from 21 eyes of 12 cases in the same pedigree.

The procedures used adhered to the tenets of the Declaration of Helsinki and were approved by the Medical Ethics Committee of both the Niigata University and National Institute of Sensory Organs. An informed consent was received from all the subjects for the tests.

Results

The findings of 5 generations of 1 family with OMD are shown in Figure 1. The numbered family members had the same mutation in *RP1L1* (p.Arg45Trp), and family members designated with the filled squares or filled circles were phenotypically diagnosed with OMD by routine examinations including visual field tests, FA, mfERGs, and Fourier-domain OCT. Only Patient 5 (age 60 years) had normal phenotype, although she had the *RP1L1* mutation.

The clinical characteristics and the results of ocular examinations of all the 14 family members with the *RP1L1* mutation (p.Arg45Trp) are listed in Tables 1 and 2. Family Member #5 was diagnosed as normal because she had normal mfERGs.

Among the 13 OMD patients (average age at the final examination, 57.2 ± 22.1 years), 12 complained of disturbances of central vision and 4 complained of photophobia (Table 1). Patient 1 did not report any visual disturbances in the right eye as did Patient 6 for both eyes. The visual dysfunction in these eyes was confirmed by mfERGs. For 13 patients, the age at the onset of visual difficulties varied from 6 years to 50 years with a mean of 27.3 ± 15.1 years.

All the patients were affected in both eyes, and the onset was the same in the 2 eyes except for Patients 1, 11, 12, and 14. Patient 1 first noticed a decrease in her visual acuity in her left eye at age 50 years, and she still did not have any subjective visual disturbances in her right eye 30 years later. However, a clear decrease in the mfERGs in the macular area was detected in both eyes. Patient 11 first noticed a decrease in the visual acuity in her right eye at age 47 years when the BCVA was 0.2 in the right eye and 1.2 in the left eye (Figure 2). Seven years later at age 54 years, she noticed a decrease in the vision in her left eye. Similarly, Patients 12 and 14 did not report any visual disturbances in their right eyes until 2 (Patient 12) or 8 (Patient 14) years after the onset in their left eyes.

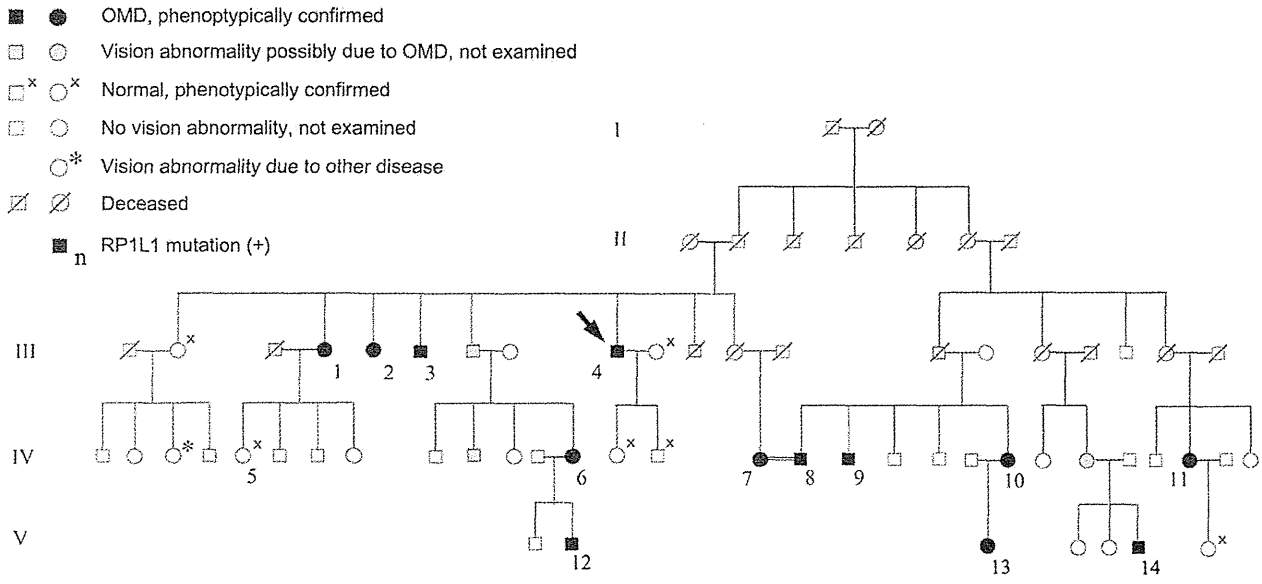

Fig. 1. Pedigree of a family with OMD. The identification number of the patients is marked beside the symbols. The proband is indicated by an arrow The open squares and circles with crosses are the relatives whose visual function was confirmed to be normal by routine examinations including Humphrey visual field tests, mfERGs, and Fourier-domain OCT Those designated by hatched squares or circles were reported to have poor vision with similar severity and onset as the other genetically confirmed OMD patients. One relative marked by an asterisk had unilateral optic atrophy because of retrobulbar neuritis.

The duration of the continuous decrease in the BCVA varied from 10 years to 30 years (mean, 15.6 ± 7.7 years) in 16 eyes of 9 adult patients. After this period, these patients reported that their vision did not decrease. Patients 2, 3, 8, and 14 complained of photophobia, and the degree of photophobia remained unchanged after the visual acuity stopped decreasing. Patients 1, 2, 4, 7, and 9 had additional disturbances of vision because of senile cataracts, and Patients 2 and 4 had bilateral cataract surgery. The visual disturbances because of the OMD were still progressing at the last examination in the left eye of Patient 11 (age 57 years), and both eyes of Patient 12 (age 20 years), Patient 13 (age 18 years), and Patient 14 (age 28 years).

Different systemic disorders were found in some of the patients; however, there did not seem to be a specific disorder, which was common to all of them (Table 1).

In the 16 eyes of 9 patients whose BCVA had stopped decreasing, the BCVA varied from 0.07 to 0.5 (Table 2). The BCVA of the left eye of Patient 6 was 0.07 because of an untreated senile cataract. If this eye is excluded, the final BCVAs of all the stationary eyes range from 0.1 to 0.5. Patient 2 had photophobia, and her BCVA measured by manually presenting Landolt rings on separate cards under room light was 0.4 in the right eye and 0.5 in the left eye, which was better than that measured by a Landolt chart of 0.3 in the right eye and 0.3 in the left eye with background illumination.

For the 13 patients whose original refractions were confirmed, 11 of 26 eyes were essentially emmetropic (<± 0.5 diopters). Both eyes of Patients 1, 3, 4, 6, and 8 and the left eye of Patient 5 were hyperopic (+0.675 to +4.625 diopters). The right eye of Patient 7, the left eye of Patient 12, and both eyes of Patient 13 were moderately myopic (−0.625 to −2.75 diopters). These results indicate that there is no specific refraction associated with OMD patients in this family.

The visual fields were determined by Goldmann perimetry or Humphrey Visual Field Analyzer. All the patients had a relative central scotoma in both eyes except for Patient 1 whose right eye was normal by Goldmann perimetry. In all cases, no other visual field abnormalities were detected during the entire course of the disease. In the patients examined shortly after the onset, a relative central scotoma was not detected by Goldman perimetry and was confirmed by static perimetry.

The fundus of all except one eye was normal. The left eye of Patient 9 had background diabetic retinopathy. At the first consultation at age 46 years, Patient 9 did not have diabetes, and the funduscopic examination and FA revealed no macular abnormalities. At the age 66 years, there were few microaneurysms in the left macula away from the fovea; however, OCT did not show any diabetic changes such as macular edema. The OMD was still the main cause of visual acuity reduction in this patient.

Six patients consented to FA, and no abnormality was detected in the entire posterior pole of the eye. It is noteworthy that both the fundus and FA of Patient 4 were normal at the age 73 years, which was >50 years

Table 1. Clinical Characteristics of the Family Members With RP1L1 Mutation (p.Arg45Trp)

Case	Age and Gender	Chief Complaint	Affected Eye	Age at Onset (Years)	Duration of Continuous Decrease in BCVA (Years)	Duration After the Onset (Years)	Systemic Disorders
1	81, F	Decreased visual acuity	Bilateral*	50	20	31	Hypertension
2	71, F	Decreased visual acuity and photophobia	Bilateral	25	25	46	Diabetes mellitus since 64 years of age
3	74, M	Decreased visual acuity and photophobia	Bilateral	30	10	44	Hyperlipidemia, angina pectoris
4	83, M	Decreased visual acuity	Bilateral	20	10	63	Hypertension, Multiple cerebral infarction at 73 years of age
5	60, F	None	—†	—	—	—	—
6	50, F	None	Bilateral*	Unknown	Unknown	Unknown	—
7	69, F	Decreased visual acuity	Bilateral	50	10	19	—
8	69, M	Decreased visual acuity and photophobia	Bilateral	28	10	41	Hypertension since 67 years of age, Surgery for ossification of the posterior longitudinal ligament at 45 years of age
9	66, M	Decreased visual acuity	Bilateral	30	15	36	Diabetes mellitus since 63 years of age
10	58, F	Decreased visual acuity	Bilateral	10	30	48	Rheumatoid arthritis since 46 years of age, Bronchiectasis since 43 years of age
11	57, F	Decreased visual acuity	Bilateral ‡	47	OD, 10, OS, still progressing	10	—
12	20, M	Decreased visual acuity	Bilateral§	14	Still progressing	6	Atopic dermatitis
13	18, F	Decreased visual acuity	Bilateral	6	Still progressing	12	—
14	28, M	Decreased visual acuity and photophobia	Bilateral¶	18	Still progressing	10	—

*Patient 1 has subjective visual disturbance only in the left eye, and Patient 6 does not have any subjective visual disturbances in both eyes. The visual dysfunction was confirmed by mfERG.

†This woman has a mutation in RP1L1, but her visual function was confirmed normal after routine examinations including mfERG.

‡This patient noticed visual disturbance only in the right eye at 47 years of age. The visual disturbance in the left eye was first noticed at 54 years of age.

§This patient noticed visual disturbance only in the left eye at 14 years of age. The visual disturbance in the right eye was first noticed at 16 years of age.

¶This patient noticed visual disturbance only in the left eye at 18 years of age. The visual disturbance in OD was first noticed at 26 years of age.

Table 2. Results of Ocular Examinations of the Family Members With RP1L1 Mutation

Case	Age and Gender	BCVA at Final Visit		Refraction (D)*		Visual Field	Fundus Appearance	FA	Full-Field ERG	Relative Amplitude in mfERG at Fovea (Ring 1/Ring 5 or Ring 6)†	Other Ocular Disorders
		OD	OS	OD	OS						
1	81, F	1.2	0.1	+4.25	+4.625	Relative central scotoma, OS	Normal, OU	Normal, OU	NE	2.34, OD, 0.60, OS	Senile cataract, OU
2	71, F	0.4	0.5	Unknown‡	Unknown‡	Relative central scotoma, OU	Normal, OU	NE	NE	Not measurable, OU	Cataract surgery, OS at 58 years of age, OD at 69 years of age, Ptosis, OU
3	74, M	0.2	0.3	+2.875	+3.375	Relative central scotoma, OU	Normal, OU	NE	NE	Not measurable, OU	Laser peripheral iridotomy, OU at 73 years of age
4	83, M	0.2	0.2	+1.0	+1.625	Relative central scotoma, OU	Normal, OU	Normal, OU	Normal ISCEV standard protocol ERG, OU	Not measurable, OU	Cataract surgery, OU at 80 years of age
5	60, F	1.2	1.2	−0.25	+0.875	Normal, OU	Normal, OU	NE	NE	4.24, OD, NE, OS	—
6	50, F	1.2	1.2	+1.0	+1.0	Relative central scotoma, OU	Normal, OU	NE	NE	2.74, OD, 2.23, OS	—
7	69, F	0.1§	0.07§	−0.625	+0.25	Relative central scotoma, OU	Normal, OU	NE	Normal ISCEV standard protocol ERG, OU	Not measurable, OU	Senile cataract, OU
8	69, M	0.1	0.1	+1.125	+0.675	Relative central scotoma, OU	Normal, OU	NE	Normal ISCEV standard protocol ERG, OU	1.01, OD, 1.30, OS	—

Table 2. (Continued)

Case	Age and Gender	BCVA at Final Visit		Refraction (D)*		Visual Field	Fundus Appearance	FA	Full-Field ERG	Relative Amplitude in mfERG at Fovea (Ring 1/Ring 5 or Ring 6)†	Other Ocular Disorders
		OD	OS	OD	OS						
9	66, M	0.2	0.3	+0.125	+0.125	Relative central scotoma, OU	Normal, OD Background diabetic retinopathy with microaneurysm, OS	Normal, OU	Normal mixed rod–cone responses, OU	1.21, OD1.59, OS	Senile cataract, OU
10	58, F	0.1	0.1	+0.5	+0.375	Relative central scotoma, OU	Normal, OU	NE	Normal cone responses, OU	Not measurable, OU	—
11	57, F	0.1	0.4	+0.5	0.0	Relative central scotoma, OU	Normal, OU	Normal, OU	Normal ISCEV standard protocol ERG, OU	Not measurable, OU	—
12	20, M	0.3	0.3	−0.375	−0.75	Relative central scotoma, OU	Normal, OU	Normal, OU	Normal ISCEV standard protocol ERG, OU	0.98, OD1.03, OS	—
13	18, F	0.2	0.15	−1.625¶	−2.75¶	Relative central scotoma, OU	Normal, OU	Normal, OU	Normal ISCEV standard protocol ERG, OU	Not measurable, OU	—
14	28, M	1.0	0.6	−0.25	−0.25	Relative central scotoma, OU	Normal, OU	NE	Normal ISCEV standard protocol ERG, OU	1.63, OD, 0.66, OS	—

D, diopter; ISCEV, International Society of Clinical Electrophysiology and Vision, NE, not examined.
*Spherical equivalents at the initial visit.
†The responses of Ring 1 were extinguished and the N1–P1 amplitudes were not measurable in Cases 2, 3, 4, 7, 10, 11, and 13.
‡This patient had already undergone cataract surgeries for both eyes at the initial visit, and no data could be obtained about the original refraction.
§This patient's visual acuity was reduced also by senile cataract.
¶The refraction of this patient was measured after instillation of cycloplegics.

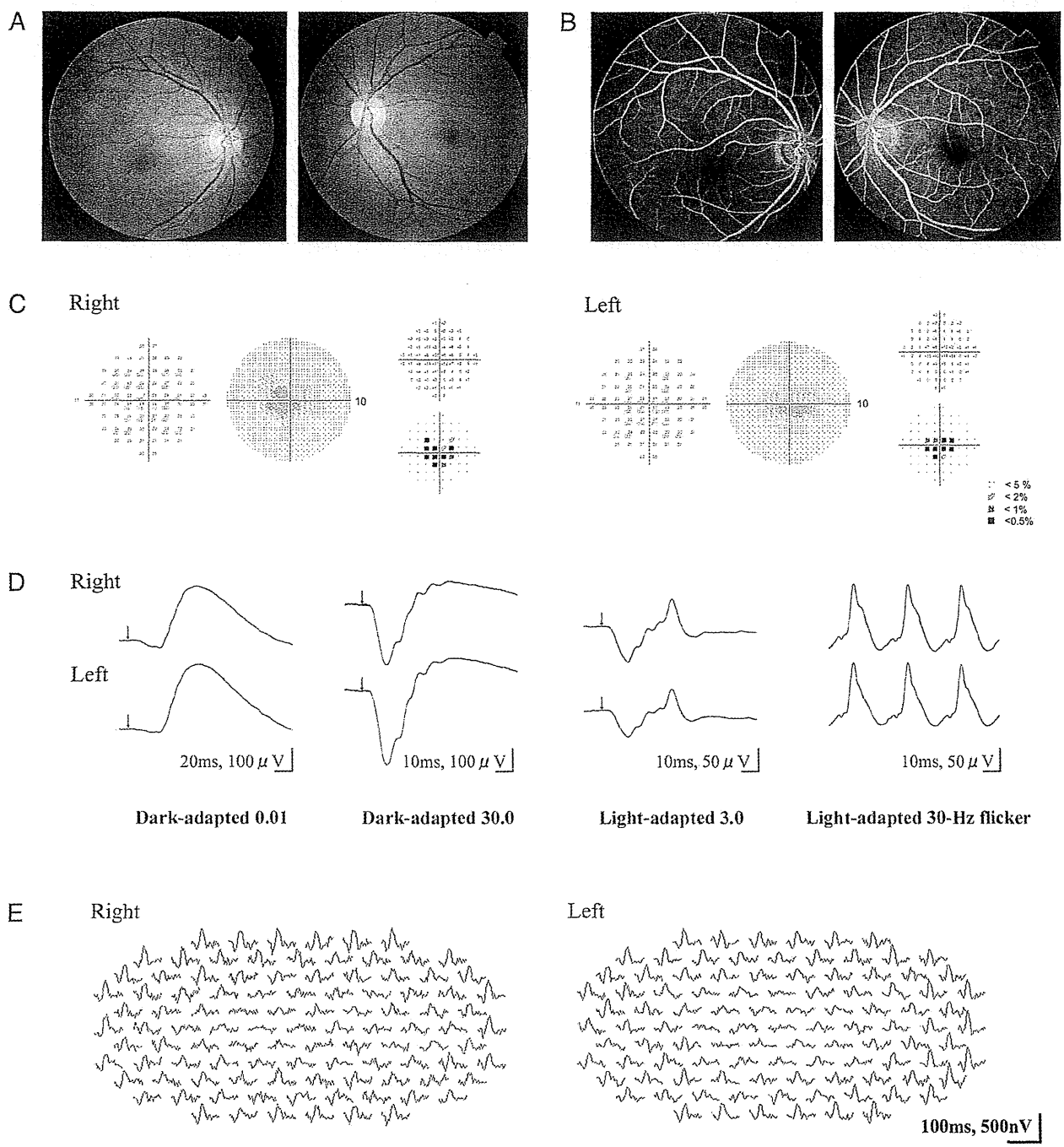

Fig. 2. Results of ocular examination of Patient 11 The data in (**A**) to (**E**) were collected 3 years after the onset of the visual disturbance at age 50 years. At this time, the patient had not noticed a decrease in the visual acuity in her left eye. The BCVA was 0.1 in the right eye and 1.2 in the right eye. **A**, and **B**. Fundus photographs and FAs showing no abnormal findings. **C**. Static visual field test (Humphrey Visual Field Analyzer, 10-2) showing relative central scotoma in both eyes. **D**. Full-field rod, mixed rod–cone, cone ERGs, and 30-Hz flicker responses. All the responses are normal in both eyes. **E**. Trace arrays of mfERGs tested with 103 hexagonal stimuli shown without spatial averaging. The responses of the central locus are extinguished in both eyes.

after the onset. This patient first noticed visual disturbances at age 20 years and was diagnosed with OMD at age 73 years. The appearance of the macula and optic disk at age 83 years was still normal >60 years after the onset of the symptoms.

Rod, mixed rod–cone, and cone full-field ERGs were recorded from 7 patients using the International Society of Clinical Electrophysiology and Vision standard protocol, and all of them showed normal rod and cone responses as in the representative case shown in

Figure 2. Only the mixed rod–cone responses were recorded from Patient 9, and only the cone responses were recorded from Patient 10, and these responses were also normal.

The amplitudes of the mfERGs were reduced in the central region of both eyes in all the 13 patients. We quantified the relative mfERG responses at the fovea by dividing the N1–P1 amplitudes of the central ring (Ring 1) by those in the outermost eccentric ring (Ring 5 in cases of 61 stimuli and Ring 6 in cases of 103 stimuli) in 13 OMD patients and 1 normal family member (Case 5) with the *RP1L1* mutation (Table 2).[4] Among the 26 eyes of the 13 OMD patients, the N1–P1 amplitudes of the central locus were measurable in 12 eyes in 6 cases tested with the 61 stimuli. The ratio of the amplitudes of Ring 1/Ring 5 in these OMD patients ranged from 0.60 to 2.74 (average of normals: 4.34 ± 0.67, n = 20). In 6 eyes tested with 61 stimuli and all the 8 eyes tested with 103 stimuli, the responses in the central locus were extinguished and the amplitudes were not measurable (see examples in Figure 2E). The ratio of the amplitudes of Ring 1/Ring 5 in a normal family member (Case 5, right eye) was 4.24, which was within the normal range.

The results of routine ocular examinations in Patient 11 at the age 50 years, when she did not have any visual disturbances in her left eye, are shown in Figure 2. The BCVA was 0.1 in the right eye and 1.2 in the left eye. The fundus and FA were normal in both eyes. Humphrey visual field tests (SITA Standard and pattern deviation 10-2) showed a relative central scotoma in both eyes. The full-field rod, mixed rod–cone, cone, and 30-Hz flicker ERGs were normal in both eyes. The mfERGs were reduced in and around the region of the central scotoma in both eyes. The Humphrey visual field test (30-2) did not detect a central scotoma in either eye (data not shown). The findings in the left eye of this patient are typical of the early stage of the OMD, where the dysfunction of the foveal region could be clearly detected in the mfERGs even though the subjective visual disturbance was almost undetectable.

Spectral-domain OCT images were recorded from 11 family members with the *RP1L1* mutation. The outer retinal structure was considered to be normal when the external limiting membrane, photoreceptor inner/outer segment (IS/OS) line, cone outer segment tip (COST) line, and retinal pigment epithelium (RPE) were clearly detected in the OCT images (Figure 3A).[11,23]

The OCT images of 5 representative OMD patients are aligned in the order of years after the onset in Figure 3B. The right eye of Case 1, which had electrophysiologically confirmed macular dysfunction but did not have subjective visual disturbances, showed a normal IS/OS line and COST line but only at the foveal center (asterisk in Figure 3B, ①). However, in the parafoveal region, the IS/OS line was blurred and the COST line could not be observed (arrowheads in Figure 3B, ①).

In the right eye of Case 11, the OCT images which were taken 10 years after the onset showed that the IS/OS line at the fovea was very blurred and thick but not disrupted. The COST line could not be observed in the macular area. In the perimacular region that had normal visual function, all the outer retinal structures were seen to be normal (Figure 3B, ②). Similar findings were observed in the left eye of Case 1 and the right eye of Case 8 (Figure 3B, ③ and ④).

In the right eye of Case 4, which was examined 63 years after the onset, the IS/OS line was disrupted at the fovea. The COST line could not be observed in the macula but was still visible in the perimacular region. The external limiting membrane and RPE could be observed to be normal over the entire region (Figure 3B, ⑤).

The OCT images of 2 sporadic cases of OMD without the *RP1L1* mutation are shown in Figure 3C. Both patients had a progressive central scotoma with normal-appearing fundus and normal FA. The full-field ERGs were normal but the focal macular ERGs elicited with a 10° spot were not recordable. Their OCT images, however, were not similar to those in patients with *RP1L1* mutation; the IS/OS line could be clearly observed at the fovea (Figure 3C, ①and ②), and the COST line could also be observed at the fovea, although it was slightly more blurred than in the normal cases. There was a minute disruption of the IS/OS line at the foveola in 1 case (asterisk in Figure 3C, ①).

The OCT findings in 21 eyes of 11 cases with the *RP1L1* mutation are summarized in Table 3. The examined eyes are listed in the order of years after the onset. Case 5, who was diagnosed as not having the typical characteristics of OMD, had completely normal retinal structures. In the case of OMD without subjective visual disturbances, the COST line and IS/OS line were normally observed only at the very center of the fovea (Case 1, right eye, Figure 3B, ①). In other affected cases, the COST line was not present and the IS/OS line appeared blurred in the entire fovea (Cases 14, right eye to 8). In patients with longer duration OMD, the IS/OS line was disrupted or not present as in Cases 2 and 4.

The retinal thickness at the foveola was measured as the distance from the internal limiting membrane to the inner border of the RPE. Considering the variation in the thickness in normals, we classified that the retina at the foveola was abnormally thin when the thickness was <160 μm. All the affected eyes with disease duration ≤ 12 years had normal foveal thickness (right